APPLIED PHYSICS LETTERS **106**, 182601 (2015)

Reducing intrinsic loss in superconducting resonators by surface treatment and deep etching of silicon substrates

A. Bruno, G. de Lange, S. Asaad, K. L. van der Enden, N. K. Langford, and L. DiCarlo
QuTech Advanced Research Center and Kavli Institute of Nanoscience, Delft University of Technology, Lorentzweg 1, 2628 CJ Delft, The Netherlands

(Received 13 February 2015; accepted 17 April 2015; published online 4 May 2015)

We present microwave-frequency NbTiN resonators on silicon, systematically achieving internal quality factors above 1 M in the quantum regime. We use two techniques to reduce losses associated with two-level systems: an additional substrate surface treatment prior to NbTiN deposition to optimize the metal-substrate interface and deep reactive-ion etching of the substrate to displace the substrate-vacuum interfaces away from high electric fields. The temperature and power dependence of resonator behavior indicate that two-level systems still contribute significantly to energy dissipation, suggesting that more interface optimization could further improve performance. © *2015 AIP Publishing LLC*. [http://dx.doi.org/10.1063/1.4919761]

Superconducting coplanar waveguide (CPW) microwave resonators are crucial elements in photon detectors,[1] quantum-limited parametric amplifiers,[2,3] and narrow-band filters,[4] as well as read-out, interconnect and memory elements in quantum processors based on circuit quantum electrodynamics.[5] They also play a critical role in hybrid devices, connecting superconducting circuits with micro- and nanomechanical resonators[6,7] and solid-state spins.[8,9] In many quantum science and technology applications, resonators must operate in the quantum regime, requiring low temperatures to reach the ground state (thermal energy $k_B T$ small compared to the photon energy at resonance, hf_r) and single-photon excitation levels. Under these conditions, however, internal quality factors (Q_is) are typically substantially lower than their high-temperature or high-power values.

In the quantum regime, the dominant loss mechanism for high-Q superconducting resonators can be attributed to parasitic two-level systems (TLSs) in the dielectrics.[10,11] TLSs may reside in the bulk substrate,[11] as well as in the metal-substrate, metal-vacuum, and substrate-vacuum interfaces[10,12–18] where electric fields may be large (see Ref. 19 and references therein for a recent review of material-related loss in superconducting circuits). Interface TLSs are common by-products of the fabrication process, often introduced by impurities associated with substrate surfaces[20,21] and etching chemistry.[22] The best resonators reported to date[15] ($Q_i = 1.72$ M at 6 GHz) are fabricated by epitaxially growing aluminum on sapphire substrates following careful surface preparation (high-temperature annealing in an oxygen atmosphere). For CPW resonators on silicon (Si) substrates, achieving $Q_i > 1$ M in the quantum regime has proven challenging, with the best resonators reported in Ref. 23. Nevertheless, silicon is a highly versatile substrate with well understood interfaces; the many available microfabrication techniques developed for other applications make it appealing for pursuing low-loss quantum devices.

In this letter, we present silicon-based, gigahertz-frequency CPW resonators with Q_i systematically above 1 M in the quantum regime, fabricated from niobium titanium nitride (NbTiN) superconducting films. This performance is reached by optimizing two aspects of the fabrication. First, the substrate surface is treated with hexamethyldisilazane (HMDS) immediately prior to metal deposition to reduce losses associated with the metal-substrate interface. Second, we employ highly anisotropic deep reactive-ion etching (DRIE) of the substrate to displace lossy substrate-vacuum interfaces away from regions of high electric field. We obtain the best performance by combining both techniques, reaching 2 M in the quantum regime.

Resonator fabrication starts with surface preparation of high-resistivity ($\rho = 150\,\mathrm{k\Omega}$ cm) Si ⟨100⟩ substrates (Topsil float zone high-purity silicon, FZ-HPS) for deposition of the superconducting film. We choose NbTiN as the

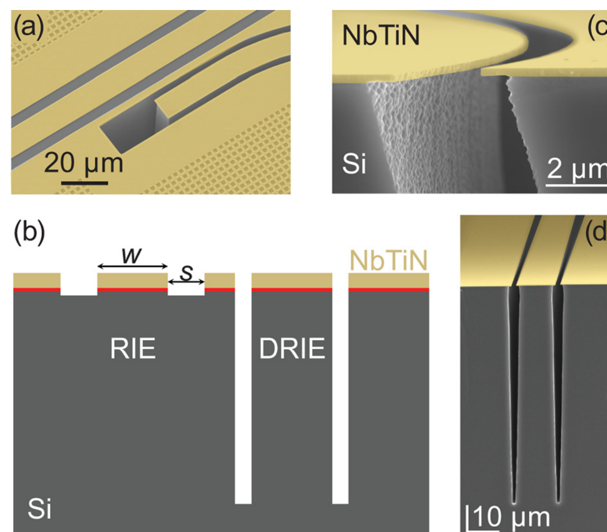

FIG. 1. False-colored scanning electron micrographs of CPW resonators and their cross sections. (a) Capacitive coupling of a RIE feedline to a DRIE resonator. (b) Schematic cross section of RIE and DRIE CPW resonators (vertical axis not to scale) in a NbTiN thin film (gold shading) on a Si substrate (grey). The treated substrate-metal interface is highlighted in red. RIE (DRIE) etches ~150 nm (~80 μm) into the substrate. (c) Cross section of a DRIE resonator near the surface, showing the metallization (300 nm), Si underetch (~1 μm) and sidewall roughness (~100 nm). (d) Cross section of DRIE resonator, showing the high etch anisotropy and depth (~80 μm).

 © 2015 AIP Publishing LLC

This article is copyrighted as indicated in the article. Reuse of AIP content is subject to the terms at: http://scitation.aip.org/termsconditions. Downloaded to IP: 131.180.131.242 On: Tue, 01 Sep 2015 13:39:49

superconductor for its high-quality metal-vacuum interface.[14] Because we define the resonators via etching of the metal film rather than lift-off, we can apply surface treatments immediately prior to metal deposition to optimize the substrate-metal interface. The substrate surface quality depends on its physical condition (e.g., roughness), chemical composition (e.g., presence of native oxides or nitrides), and chemical cleanliness (e.g., absence of polymers or metals). For example, thin (∼2 nm) amorphous native silicon oxide layers are known to host a considerable density of TLSs.[11,13] Various adsorbates can in turn attach to the native oxides. For instance, hydroxyl groups (-OH) couple to dangling bonds on the substrate surface and build a layer of silanol groups (Si-OH). This silanol layer is also hydrophilic, and thus adsorbs additional water and dipolar molecules. We first remove lossy oxides from the surface following the standard practice of dipping the Si substrate in a 1:7 buffered solution of hydrofluoric acid (HF) for 2 min, which both etches away surface oxides and terminates the Si surface with hydrogen.[20,24] We then include an additional step immediately following the HF dip, placing the substrate on a hot plate for 2 min at 110 °C while exposing the surface to an HMDS-nitrogen(N_2) atmosphere. HMDS is an organosilicon compound most commonly used as a primer to improve resist adhesion, to create hydrophobic surfaces, and to prepare substrates in the growth of high-mobility graphene.[25] XPS surface analysis of substrates immediately after these treatments revealed an absence of Si-O bonds for both the HF-only and HF + HMDS cases.[24] After also analyzing the dynamics of surface re-oxidation,[24] we conclude that the Si surface does not re-oxidize either during the HMDS treatment or loading of the substrate in the high-vacuum chamber for NbTiN deposition. Following surface preparation, NbTiN is sputtered in a reactive atmosphere of argon (Ar: 100 sccm) and nitrogen (N_2: 5.2 sccm) at 6 mTorr and 450 W (DC). The films are 160 or 300 nm thick,[24] with a typical critical temperature of 15.5 K and $\rho = 110\,\mu\Omega$ cm (measured at room temperature).

We next aim to reduce intrinsic losses associated with the substrate-vacuum interface. We employ DRIE of the exposed Si substrate using the Bosch process[26] to move the substrate-vacuum interface away from regions of high electric field (Figs. 1(a) and 1(b)). The Bosch process, consisting of alternating etching and passivation steps, is highly tunable, with variable etch depth, under-etch, sidewall roughness and passivation.[27] The DRIE resonators presented here have $\sim 1\,\mu$m under-etch below the edges of the metal regions, side-wall scalloping with ∼100 nm features (Fig. 1(c)), and a polymeric fluorocarbon layer uniformly deposited on the exposed Si surfaces during the etching process.

We now describe a recipe which allows fabrication of both RIE and DRIE structures on the same chip. First, the NbTiN films are patterned using e-beam lithography and RIE to define feedlines and standard resonators. Next, an 8-μm-thick layer of AZ 9216 photoresist is spun, followed by 25 nm of sputtered tungsten and a layer of PMMA A4. After e-beam patterning and developing the PMMA, a short RIE step is used to etch the tungsten, creating a metallic mask for a 1-h anisotropic O_2-plasma ashing of the AZ resist. We then deep-etch the Si substrate, alternating between etching using an inductively coupled plasma (ICP) of SF_6 gas (20 mTorr, 2200 W, 7 s) and fluorocarbon passivation with an ICP of C_4F_8 (2 mTorr, 1200 W, 2 s). The thick AZ layer allows etching to a depth of 80 μm (Fig. 1(d)) and 500 nm minimum feature size. The highly anisotropic O_2 etch of the thick AZ resist enables <100 nm misalignment between DRIE and RIE structures, limited only by the precision of e-beam patterning for the top PMMA layer. After the DRIE process, the residual AZ resist is cleaned in PRS-3000 photoresist stripper for 30 min at 88 °C, leaving no residuals visible under either optical or electron microscopy.

For the devices in this study, we employ quarter-wave CPW resonators with center conductor width fixed to $W = 12\,\mu$m and separation S between the center conductor and ground planes set to give a transmission-line impedance close to 50 Ω. For RIE resonators, we set $S = 5\,\mu$m, taking into account $\epsilon_r = 11.9$ for the silicon substrate and a kinetic inductance fraction of ∼16%. For DRIE resonators, we decreased S to 2 μm to compensate for the reduced effective dielectric constant. From resonator frequencies, we estimate a DRIE resonator impedance of ∼62 Ω. The resonators are capacitively coupled to a common feedline with a target coupling quality factor Q_c between 700 K and 1 M. After dicing and final cleaning in N-Methyl-2-pyrrolidone (NMP), the devices are mounted in a copper PCB with Apiezon N grease, wire-bonded and anchored to the mixing chamber plate of a dilution refrigerator routinely employed for characterizing resonators (and qubits) in the quantum regime.[24]

We quantify resonator performance by measuring their power and temperature-dependent resonance lineshapes. Specifically, we measure the complex-valued feedline transmission S_{21} near the fundamental frequencies f_r of each coupled resonator and fit the data[24,28] to extract f_r and Q_i. Here, we report measurements for our best resonators, fabricated using both surface treatment and DRIE techniques (see supplementary material[24] for other devices). We show Q_i as a function of excitation power for four HMDS-DRIE resonators with fundamental frequencies $f_r = 2.75$–6.41 GHz (Fig. 2). All resonators show $Q_i > 1$ M in the quantum regime (average intraresonator photon number $\langle n_{ph}\rangle \sim 1$, $T \sim 15$ mK). However, we observe further increases in Q_i

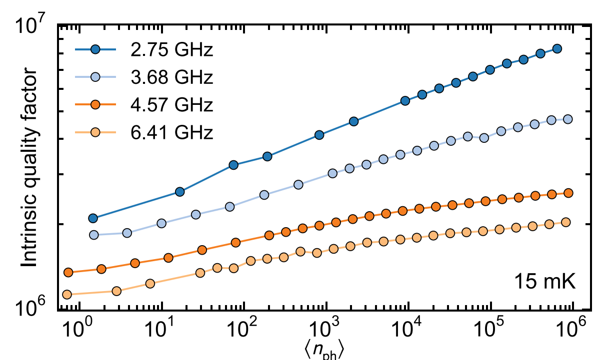

FIG. 2. Intrinsic quality factors of four DRIE resonators measured at 15 mK. Q_i is extracted from measurements of complex-valued feedline transmission. The DRIE resonators (NbTiN thickness ∼300 μm, central conductor width $W = 12\,\mu$m, and gap $S = 2\,\mu$m) have fundamental frequencies ranging from 2.75 to 6.41 GHz. The best-fit values of f_r, Q_i, and Q_c are used to convert the calibrated input power to $\langle n_{ph}\rangle$.[24] All resonators show $Q_i > 1$ M in the quantum regime, with higher Q_is attainable for higher $\langle n_{ph}\rangle$ and lower f_r. Error bars are smaller than the symbol size.

This article is copyrighted as indicated in the article. Reuse of AIP content is subject to the terms at: http://scitation.aip.org/termsconditions. Downloaded to IP: 131.180.131.242 On: Tue, 01 Sep 2015 13:39:49

(up to 4 times at 2.75 GHz) as the resonator is populated with more photons.[29] This suggests that the low-power limits for the resonators are still significantly influenced by TLSs. We also observe a systematic increase in Q_i with decreasing f_r, explanations for which include the decrease in TLS polarization at lower frequencies and the decrease in radiation losses at longer wavelengths.

To study the effects of TLS polarization, we acquire the power dependent Q_i of the 2.75 GHz resonator for $T = 15$–400 mK (Fig. 3(a)). For all excitation powers, Q_i increases monotonically with temperature over this range, and higher temperatures make Q_i less power dependent, with the factor of 4 change at 15 mK dropping to a factor of only 1.5 at around 400 mK. We therefore conclude that TLSs still provide significant loss in the quantum regime and attribute the increase of Q_i with temperature to thermal depolarization of TLSs.

A more detailed temperature dependence is acquired by measuring S_{21} around 2.75 GHz at fixed $\langle n_{ph}\rangle \sim 10^5$ while the device is continuously cooled from 900 to 15 mK. Fitting S_{21} as before, we extract Q_i and f_r. Initially, Q_i increases during cooling due to decreasing quasiparticle-induced loss,[13] before reaching a maximum value of ∼8.6 M at $T \sim 0.4$ K (Fig. 3(b)). Below 0.4 K, Q_i decreases again as increasing TLS polarization leads to greater absorption of resonator photons.

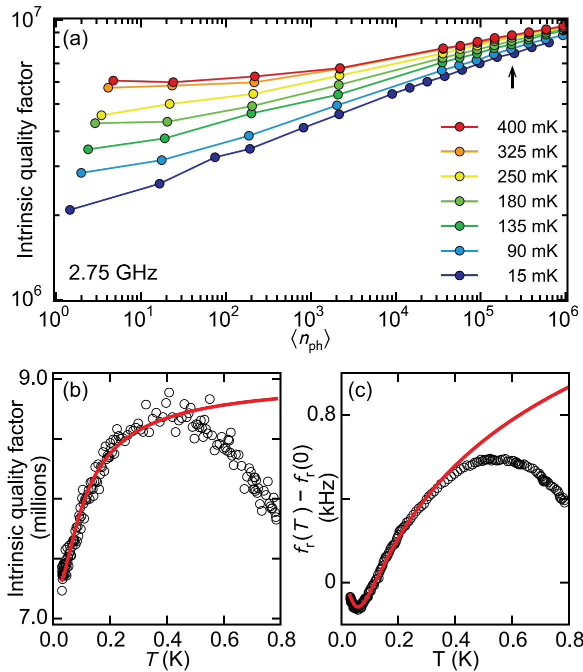

FIG. 3. Temperature dependence of 2.75 GHz DRIE resonator. (a) Power dependence of Q_i measured for $T = 15$–400 mK. At high powers, Q_i is similar for all T, but temperature dependence increases for lower $\langle n_{ph}\rangle$. (b) and (c) Resonator probed at fixed $\langle n_{ph}\rangle \sim 10^5$ (black arrow in (a)) while device is cooled from 900 to 15 mK (plotted against mixing chamber temperature). Both Q_i (b) and Δf (c) show non-monotonic temperature dependence. We attribute the initial increase in Q_i and Δf (as temperature decreases) to a decrease in quasiparticle-related loss. At $T \lesssim 400$ mK, Q_i and Δf begin to decrease as TLS-related losses increase. Data fitting to a simple model[30] for Δf (solid red line in (c); Eq. (1)) show that, in this regime, the behaviour is dominated by the T-dependence of TLS polarization. Modifying the related TLS model for Q_i to account for high excitation power (solid red line in (b); Eq. (2)) provides estimates for a TLS polarization fraction at $\langle n_{ph}\rangle \sim 10^5$ of ∼4%, and a background (non-TLS) loss of ∼1/(9 M) which is consistent with high-power Q_i s from (a).

Resonator loss from TLSs predominantly depends on their density of states at f_r and the applied microwave power.[19,31] The continuing power dependence of Q_i at single-photon levels (Fig. 2) shows that even at these low powers, resonant TLSs are still being depolarized by the incident microwaves, suggesting a significant loss contribution from TLSs with low saturation powers or, equivalently, long lifetimes. Because Q_i does not reach its low-power baseline, this limits the usefulness of the Q_i measurements in quantifying the TLS-related loss. An alternative way to probe the effect of TLSs is to study the temperature dependence of f_r. Unlike loss, the dispersive shift of the resonator also depends on non-resonant TLSs that are not saturated by the applied microwaves.[30] Their influence on f_r can therefore be measured even at high $\langle n_{ph}\rangle$. Figure 3(c) shows the temperature dependence of the resonator frequency shift $\Delta f_r(T) = f_r(T) - f_r(0)$ extracted from the same data as Fig. 3(b). The local maximum in Δf_r at $T \sim 500$ mK again reflects the loss-dependent pull of the resonator, but unlike Q_i, Δf_r is not monotonic below this temperature.

The low-temperature behavior of Δf_r is well described by a two-parameter TLS model,[30]

$$\Delta f_r(T) = \frac{k}{\pi}\left[\mathrm{Re}\,\Psi\left(\frac{1}{2} + \frac{1}{2\pi i}\frac{hf_r(T)}{k_B T}\right) - \ln\left(\frac{1}{2\pi}\frac{hf_r(T)}{k_B T}\right)\right] f_r(0). \tag{1}$$

Here, Ψ is the complex digamma function, and $f_r(0)$ is the resonator frequency at $T = 0$, and $k = F\delta$ is a combined loss parameter, where δ is the loss tangent (at $T = 0$ and $\langle n_{ph}\rangle = 0$) and F is the filling factor of the TLS host material. Fitting the TLS model with k and $f_r(0)$ as free parameters (red curve in Fig. 3(c)) shows good agreement with the data for $T < 400$ mK and accurately captures the distinctive local minimum in Δf at $T \sim 60$ mK. The best-fit value $k = 6.35(4) \times 10^{-7}$ compares well with previous values found for Nb resonators on sapphire.[10] This value can also be used to predict the low-power, low-temperature limit of TLS-related loss,[30] giving $Q_i \approx 1/k \sim 1.6$ M. The ∼20% disparity with the measured single-photon Q_i (Fig. 2) fits with previous observations.[30] It arises partly because Δf_r is sensitive to TLSs over a broad frequency bandwidth, giving an estimate of average loss tangent δ which may differ from the local loss tangent inside the resonator bandwidth,[30] and partly because we do not reach a baseline value of Q_i even at the single-photon level.

We also fit an heuristic model for the low-temperature dependence of Q_i modified from Ref. 30,

$$\frac{1}{Q_i} = k_{\mathrm{eff}} \tanh\left(\frac{hf_r(T)}{2k_B T}\right) + \frac{1}{Q_{\mathrm{other}}}. \tag{2}$$

Here, we introduce two *ad hoc* fitting parameters, a modified loss parameter k_{eff} to account for the reduced TLS polarization at high excitation power, and an extra, fixed loss term $1/Q_{\mathrm{other}}$ which accounts for the non-TLS-related loss which becomes significant as temperature increases. This fit also agrees well with the data at $T \lesssim 0.4$ K (red curve in

This article is copyrighted as indicated in the article. Reuse of AIP content is subject to the terms at: http://scitation.aip.org/termsconditions. Downloaded to IP: 131.180.131.242 On: Tue, 01 Sep 2015 13:39:49

Fig. 3(b)), with best-fit values of $k_{\rm eff} = 2.64(4) \times 10^{-8}$ and $Q_{\rm other} = 9.02(2) \times 10^{6}$. The ratio $k_{\rm eff}/k_{\rm fit} \sim 0.04$ provides an estimate of the TLS polarization fraction still remaining at $\langle n_{\rm ph} \rangle \sim 10^{5}$, while $Q_{\rm other}$ is consistent with the high-power $Q_{\rm i}$s measured in Fig. 3(a).

In conclusion, we have demonstrated few-GHz CPW resonators on silicon with intrinsic quality factors exceeding one million in the quantum regime, achieved through surface treatment and substrate etching. Our results suggest that these resonators exhibit a significant reduction in TLS-related losses, but the temperature and power dependences indicate that TLSs are still an important source of energy loss. This offers the opportunity for further improvements by interface optimization, perhaps pushing quantum-regime resonator performance towards the high-power limit with $Q_{\rm i}$s approaching 10 M at lower frequencies. Since we have only partially explored the available parameter ranges in this study, future efforts will include optimizing the DRIE recipe and studying the effects of etch depth, side-wall roughness, and under-etch on resonator losses. Finally, these surface-treatment and DRIE techniques can be directly applied to the fabrication of superconducting qubits in integrated circuits, offering a path towards longer qubit coherence times.

We thank T. M. Klapwijk, P. J. de Visser, and D. J. Thoen for discussions and high-quality NbTiN films, and V. de Rooij and E. van Veldhoven for the XPS investigation. We acknowledge funding from the Dutch Organization for Fundamental Research on Matter (FOM) and a Marie Curie Career Integration Grant (L.D.C.).

[1]P. K. Day, H. G. LeDuc, B. A. Mazin, A. Vayonakis, and J. Zmuidzinas, Nature **425**, 817 (2003).
[2]M. A. Castellanos-Beltran, K. D. Irwin, G. C. Hilton, L. R. Vale, and K. W. Lehnert, Nat. Phys. **4**, 929 (2008).
[3]N. Bergeal, F. Schackert, M. Metcalfe, R. Vijay, V. E. Manucharyan, L. Frunzio, D. E. Prober, R. J. Schoelkopf, S. M. Girvin, and M. H. Devoret, Nature **465**, 64 (2010).
[4]A. Endo, C. Sfiligoj, S. J. C. Yates, J. J. A. Baselmans, D. J. Thoen, S. M. H. Javadzadeh, P. P. van der Werf, A. M. Baryshev, and T. M. Klapwijk, Appl. Phys. Lett. **103**, 032601 (2013).
[5]A. Blais, R.-S. Huang, A. Wallraff, S. M. Girvin, and R. J. Schoelkopf, Phys. Rev. A **69**, 062320 (2004).
[6]C. A. Regal, J. D. Teufel, and K. W. Lehnert, Nat. Phys. **4**, 555 (2008).
[7]J. D. Teufel, C. A. Regal, and K. W. Lehnert, New J. Phys. **10**, 095002 (2008).
[8]Y. Kubo, F. R. Ong, P. Bertet, D. Vion, V. Jacques, D. Zheng, A. Dréau, J.-F. Roch, A. Auffeves, F. Jelezko *et al.*, Phys. Rev. Lett. **105**, 140502 (2010).
[9]R. Amsüss, C. Koller, T. Nöbauer, S. Putz, S. Rotter, K. Sandner, S. Schneider, M. Schramböck, G. Steinhauser, H. Ritsch *et al.*, Phys. Rev. Lett. **107**, 060502 (2011).
[10]J. Gao, M. Daal, A. Vayonakis, S. Kumar, J. Zmuidzinas, B. Sadoulet, B. A. Mazin, P. K. Day, and H. G. Leduc, Appl. Phys. Lett. **92**, 152505 (2008).
[11]A. D. O'Connell, M. Ansmann, R. C. Bialczak, M. Hofheinz, N. Katz, E. Lucero, C. McKenney, M. Neeley, H. Wang, E. M. Weig *et al.*, Appl. Phys. Lett. **92**, 112903 (2008).
[12]M. R. Vissers, J. Gao, D. S. Wisbey, D. A. Hite, C. C. Tsuei, A. D. Corcoles, M. Steffen, and D. P. Pappas, Appl. Phys. Lett. **97**, 232509 (2010).
[13]R. Barends, H. Hortensius, T. Zijlstra, J. Baselmans, S. Yates, J. Gao, and T. Klapwijk, Appl. Phys. Lett. **92**, 223502 (2008).
[14]R. Barends, N. Vercruyssen, A. Endo, P. De Visser, T. Zijlstra, T. Klapwijk, and J. Baselmans, Appl. Phys. Lett. **97**, 033507 (2010).
[15]A. Megrant, C. Neill, R. Barends, B. Chiaro, Y. Chen, L. Feigl, J. Kelly, E. Lucero, M. Mariantoni, P. J. J. O'Malley *et al.*, Appl. Phys. Lett. **100**, 113510 (2012).
[16]S. J. Weber, K. W. Murch, D. H. Slichter, R. Vijay, and I. Siddiqi, Appl. Phys. Lett. **98**, 172510 (2011).
[17]M. S. Khalil, F. Wellstood, and K. D. Osborn, IEEE Trans. Appl. Supercond. **21**, 879 (2011).
[18]K. Geerlings, S. Shankar, E. Edwards, L. Frunzio, R. J. Schoelkopf, and M. H. Devoret, Appl. Phys. Lett. **100**, 192601 (2012).
[19]W. D. Oliver and P. B. Welander, MRS Bull. **38**, 816 (2013).
[20]D. S. Wisbey, J. Gao, M. R. Vissers, F. C. da Silva, J. S. Kline, L. Vale, and D. P. Pappas, J. Appl. Phys. **108**, 093918 (2010).
[21]C. M. Quintana, A. Megrant, Z. Chen, A. Dunsworth, B. Chiaro, R. Barends, B. Campbell, Y. Chen, I. Hoi, E. Jeffrey *et al.*, Appl. Phys. Lett. **105**, 062601 (2014).
[22]W. Chen, D. A. Bennett, V. Patel, and J. E. Lukens, Supercond. Sci. Technol. **21**, 075013 (2008).
[23]M. Sandberg, M. R. Vissers, J. S. Kline, M. Weides, J. Gao, D. S. Wisbey, and D. P. Pappas, Appl. Phys. Lett. **100**, 262605 (2012).
[24]See supplementary material at http://dx.doi.org/10.1063/1.4919761 for additional data.
[25]M. Lafkioti, B. Krauss, T. Lohmann, U. Zschieschang, H. Klauk, K. v. Klitzing, and J. H. Smet, Nano Lett. **10**, 1149 (2010).
[26]F. Laermer and A. Schilp, "Method of Anisotropically Etching Silicon," U.S. patent 498,312 (1996).
[27]Z. Liu, Y. Wu, B. Harteneck, and D. Olynick, Nanotechnology **24**, 015305 (2013).
[28]M. S. Khalil, M. J. A. Stoutimore, F. C. Wellstood, and K. D. Osborn, J. Appl. Phys. **111**, 054510 (2012).
[29]R. Barends, N. Vercruyssen, A. Endo, P. J. De Visser, T. Zijlstra, T. M. Klapwijk, P. Diener, S. J. C. Yates, and J. J. A. Baselmans, Appl. Phys. Lett. **97**, 023508 (2010).
[30]D. P. Pappas, M. R. Vissers, D. S. Wisbey, J. S. Kline, and J. Gao, IEEE Trans. Appl. Supercond. **21**, 871 (2011).
[31]W. A. Phillips, Rep. Prog. Phys. **50**, 1657 (1987).

This article is copyrighted as indicated in the article. Reuse of AIP content is subject to the terms at: http://scitation.aip.org/termsconditions. Downloaded to IP: 131.180.131.242 On: Tue, 01 Sep 2015 13:39:49